NASA TECHNICAL NOTE

NASA TN D-4645

TRANSITION AND FLOW REATTACHMENT BEHIND AN APOLLO-LIKE BODY AT MACH NUMBERS TO 9

by Robert L. Kruse

Ames Research Center
Moffett Field, Calif.

NATIONAL AERONAUTICS AND SPACE ADMINISTRATION • WASHINGTON, D. C. • JULY 1968

TRANSITION AND FLOW REATTACHMENT BEHIND AN APOLLO-LIKE BODY AT MACH NUMBERS TO 9

By Robert L. Kruse

Ames Research Center
Moffett Field, Calif.

NATIONAL AERONAUTICS AND SPACE ADMINISTRATION

For sale by the Clearinghouse for Federal Scientific and Technical Information
Springfield, Virginia 22151 – CFSTI price $3.00

TRANSITION AND FLOW REATTACHMENT BEHIND AN APOLLO-LIKE BODY AT MACH NUMBERS TO 9

By Robert L. Kruse

Ames Research Center

SUMMARY

Transition from laminar to turbulent flow in the near wake of a bluff body has been studied in the Ames Pressurized Ballistic Range. The location of transition and the reattachment of the separated flow have been determined from shadowgraphs and have been correlated on the basis of Mach number, Reynolds number, and angle of attack. The Mach numbers ranged from 1 to 9, the Reynolds numbers (based on body diameter) from 0.25×10^6, to 5×10^6, and the angles of attack from 0° to 25°.

INTRODUCTION

The flow beyond the corners of nearly flat-faced entry bodies with convergent afterbodies, such as the Apollo, determines the heat transfer to the afterbody. It can, in principle, be either separated from or attached to the afterbody, and laminar or turbulent. If separated, it may reattach somewhere along the convergent afterbody and cause a local peak in the afterbody heat transfer. Some of the many variables affecting this behavior are Mach number, Reynolds number, angle of attack, surface roughness, corner radius, mass injection, and heat transfer. There is no theoretical basis for predicting this flow behavior.

The problem of afterbody flow separation and reattachment is coupled to the problem of laminar-turbulent transition. The separation behavior is different for laminar and turbulent boundary layers. Furthermore, the behavior of the boundary layer as well as its appearance after it separates from the front-face corner is evidence of the condition of the boundary layer on the face, where it is also important to heat transfer. Hence, information on the boundary-layer transition obtained herein may aid in indicating conditions for which laminar flow may be expected to persist to the edge of the front face.

Experimental observation of the flow over the afterbody from shadowgraphs (see, e.g., ref. 1) has, in the past, been perhaps the most definitive technique of determining models of the flow field for calculating full-scale heating. The present investigation was undertaken by this technique to extend the information available to broader ranges of Reynolds number, Mach number, and angle of attack, and to correlate the flow behavior in terms of these parameters.

The experiments cover a range of Mach numbers from 1 to 9, Reynolds numbers based on free-stream properties and diameter from 0.25×10^6 to 5×10^6,

angles of attack up to 25°, and model diameters from 0.6 to 3 cm. A portion of the data presented was taken from shadowgraphs of the same configuration obtained in the investigations of references 1 and 2.

SYMBOLS

d	body diameter, cm
L	afterbody slant length, cm
$\overline{L}$	distance to reattachment aft of model corner along afterbody windward meridian, cm
M	free-stream Mach number
p	free-stream static pressure, atm
r	radius, cm
$R_{\infty d}$	Reynolds number based on free-stream conditions and body diameter
R_{e_θ}	Reynolds number based on inviscid flow properties at boundary-layer edge and boundary-layer-momentum thickness at front-face corner
R_{2_d}, R_{2_x}	Reynolds number based on flow properties downstream of the normal part of the bow-shock wave and dimension d or x
s	distance to transition aft of model corner, windward or leeward meridian, cm
x	streamline distance from stagnation point to corner at junction of front face and afterbody (See fig. 8. The stagnation point was assumed to be the forwardmost point on the body.)
α	angle of attack, deg

TEST DESCRIPTION

Model

The configuration used in the investigation (fig. 1) has a spherical-segment face with a radius of curvature equal to the frontal diameter, and a conical afterbody. The models were made of solid phosphor bronze or 7075-T6 aluminum, and had diameters of 1 cm and 3 cm, respectively.

No special care was taken in polishing the surfaces of most models. The front faces had circumferential scratches about 1 micron deep, caused by an emery polish after the machining operation. One model, 3 cm in diameter, with the face polished to a surface roughness of about 0.3 micron, was used to check the possible effect of surface roughness on the position of boundary-layer transition.

Test Facility

The investigation was conducted in the Ames Pressurized Ballistic Range, a facility 62 meters long and equipped with 24 spark-shadowgraph stations, each utilizing a conical projection light system. The facility can be evacuated or pressurized. The models were launched from smooth-bore guns into still air at velocities less than that at which radiation from their shock layers would fog the shadowgraph film (nominally 3.6 km/sec).

The flow field observed in each shadowgraph was studied to determine the state of the boundary layer in the near wake, as well as how the boundary-layer separation and reattachment characteristics were affected by angle of attack, Reynolds number, and Mach number. Since the models decelerated considerably, each test yielded results for ranges of free-stream Mach number and Reynolds number.

Boundary-Layer Transition and Shadowgraph Interpretation

The condition of the boundary layer on the model front face and in the separated streamline downstream of the model corners can usually be inferred from the shadowgraph. A detailed discussion of the criteria used for interpreting the shadowgraphs of this investigation is given in the appendix.

RESULTS AND DISCUSSION

Discussion of Typical Shadowgraphs

The effect of Reynolds number on the extent of laminar run is illustrated by figure 2. Figures 2(a) and (b) show the effect in the separated flow on the leeward meridian, while the flow on the windward meridian is laminar to reattachment. (The flight direction is nearly parallel to the horizontal reference wires and the downwash and large-scale eddy formation in the wake can be seen.) The effect on flow entirely separated over the afterbody is seen in figures 2(c) and (d).

The explicit influence of angle of attack on the wake flow is shown in figure 3. The increase in laminar run downstream of the windward corner can be seen, while the flow aft of the leeward corner was considered turbulent in all cases.

Optical distortion of the model profile resulting from the strong expansion field near the model corner makes the model corners appear cusped (see figs. 2(b) and (d) and fig. 3). This distortion was considered when the distance to transition was measured by extending the arc of the front-face profile to the conical-afterbody profile and measuring from this intersection.

Figure 3(d) shows some unusual phenomena observed in several of the shadowgraphs. The waves lying parallel to and between the model front face and bow shock wave have caused considerable speculation. Waves of this type have been observed in the past (ref. 3) in free-flight tests of blunt bodies flying through a countercurrent supersonic airstream. This is the first instance known to the author when these waves have been observed in a shadowgraph of a free-flying model in still air. A possible cause of the waves is unsteady transition from laminar-to-turbulent boundary layer on the model face. The oblique body-fixed waves emanating from the front face are believed to result from supersonic flow over surface roughness. These waves were observed in a number of shadowgraphs and begin to appear at an angular displacement of about 42° from the stagnation point (i.e., close to the sonic point).

In a few cases, fully attached flow was noted on the afterbody at angles of attack near zero, as shown in figure 4(a). On a similar flight at a slightly lower Mach number and Reynolds number (fig. 4(b)), the afterbody flow was separated.

The shadowgraphs of figures 2, 3, and 4 illustrate the relationship between the afterbody flow and the test variables. Some order is seen to exist and much of the ensuing discussion is devoted to describing the correlation of observations from shadowgraphs like these. To limit the investigation to a manageable scope, observations were restricted to the pitch plane of the configuration. To minimize crossflow effects only those shadowgraphs were used for which the angle of yaw (normal to the observation plane) was less than 5°.

Conditions for Flow Reattachment

The flight conditions (angle of attack and Mach number) at which there was reattachment of a separated boundary layer on the afterbody windward meridian are shown in figure 5 for each combination of model size and range pressure. The open symbols represent separated flow and the filled symbols represent reattachment somewhere along the afterbody. The flow was considered reattached if it turned sufficiently to produce a visible shock-wave image along the afterbody (see figs. 2(a), 2(b), 3(c), and 3(d)). In a few cases the separated flow appeared to reattach to the body near the base apex without causing a reattachment shock wave. These cases have been identified in figure 6 as "marginally attached." (A spurious double image in fig. 2(c), due to light reflecting from the shadowgraph spark source, makes the trailing shock wave appear also as a reattachment shock wave on the afterbody windward meridian. Clearly, however, in this case there was no reattachment.) The number adjacent to each filled symbol represents the percent of the afterbody

windward meridian covered by reattached flow. The relationship between angle of attack, Mach number, and percent of reattached flow observed along the windward meridian can be seen. A straight line was faired through the data points, dividing those representing separated and reattached flow. This line, which divides the data reasonably well, is common to all plots and shows that incipient reattachment is independent of Reynolds number within the range covered.

Further study of the data of figure 5 indicated that reattachment may be influenced by whether the boundary layer is laminar or turbulent immediately downstream of the corner (see, especially, the high Reynolds number points, fig. 5(d)). This led to the plot in figure 6 which includes the data of figure 5; each data point for which the flow downstream of the windward corner was turbulent is indicated by a flagged symbol. The faired line from figure 5 is also included. Another faired line is shown representing the conditions for reattachment of turbulent flow. One point at $M = 7.6$ and $\alpha = 5.5°$ does not agree with the reattachment curve. It is possible that Reynolds number does influence reattachment through its influence on transition at or ahead of the corner. But turbulent flow on the face is not a sufficient condition for attached flow on the afterbody at small angles of attack.

A few observations of flow reattachment were made on meridians other than the windward meridian in order to define the boundaries of reattached flow on the afterbody. These are shown in figure 7. Half the model afterbody surface is shown as it would appear if rolled out on a plane surface. The area covered by reattached flow is enclosed by the windward meridian and the line faired through the data points for each Mach number and angle-of-attack condition illustrated. For all cases, the flow was laminar downstream of the windward corner. While it is not possible to establish an accurate trend from the few cases shown, the locus of reattachment shows a reasonably well-defined pattern.

Occurrence of a Laminar or Turbulent Separated Boundary Layer

The data in figure 8 are the result of numerous shadowgraph observations in which the Reynolds number, R_{2_x}, is plotted against Mach number. Each data point is one of a pair. The angles of attack ranged to 25°. The faired band divides flow conditions for which some laminar flow and no laminar flow occurred in the boundary-layer downstream of the corner. Below a Mach number of about 1.7 no separated laminar flow was observed. As the Mach number increased above 1.7, laminar flow appeared in the separated streamline at the lower Reynolds numbers. Between Mach numbers 2 and 9, the limiting value of R_{2_x} for laminar flow in the wake appears to be between 250,000 and 350,000. The mean value of 300,000 will be used when subsequent reference is made to this limit.

The filled circles flagged at R_{2_x} near 5×10^5 and $M > 5$ represent observations of attached afterbody flow near zero angle of attack, as shown in figure 4(a). Attached flow of this type is reported in reference 4 on a

Mercury capsule model with a roughened face. It was believed that attached afterbody flow was the result of turbulent flow at high Reynolds numbers on the model face. Reattachment at the high Mach numbers is possibly due, in part, to heat transfer which causes the transition Reynolds number to decrease with increasing Mach number (discussed in ref. 5). The heat-transfer conditions were not varied independently of Mach number and Reynolds number. In these tests the model temperature remains substantially equal to the free-stream static temperature.

Transition in the Separated Boundary Layer

A correlation of the distance from the stagnation point to transition on the separated streamline with Reynolds number is presented in figure 9. The total distance, $x + s$, is normalized with respect to the model diameter. Presenting the distance to transition in this manner accounts for angle-of-attack effects, the total distance to transition being the same on both windward and leeward streamlines, within the accuracy of measurement. For clarity, only the windward values of $(x + s)/d$ are shown. Data near a Mach number of 3 are shown for several conditions of model size and ambient pressure, and the curve is faired through the data. It is seen that the distance to transition decreases as R_{2_d} increases. Also shown for comparison are data near Mach numbers of 4 and 8, at $R_{2_d} \approx 0.37\times10^6$. These data illustrate a phenomenon that appeared in the Mach number range from 2 to 8. The extent of laminar run appeared to increase as the Mach number increased from 2 to 4, and to decrease as the Mach number further increased from 4 to 8. The reason for this is not known.

From the auxiliary plot of x/d versus α, inset in figure 9, it is seen that when $\alpha = 0°$, $x/d = 0.52$, and s goes to zero when $R_{2_d} \approx 0.7\times10^5$. Then R_{2_x} has a value of 3.6×10^5, which compares reasonably well with the criterion determined from figure 8 for turbulent flow downstream of the corner. In figure 9, while the data points representing the polished model fall near the upper part of the group of points near $R_{2_d} = 1.1\times10^6$, no appreciable increase in length of laminar run due to reduced roughness is indicated.

Probability of Transition on Model Face

As noted earlier, the condition of the boundary layer on the face generally could not be observed directly. However, the information previously presented suggests a criterion for the onset of turbulence on the face. In figure 8, the limit for laminar flow downstream of the model corner was $R_{2_x} = 3\times10^5$. In the discussion of figure 9, it was shown that the laminar run downstream of the model corner vanished when R_{2_x} was near 3×10^5. From these observations, it might be concluded that turbulent flow does not occur on the face of the body at $R_{2_x} < 3\times10^5$. The value of R_{e_θ} at the corner, corresponding to $R_{2_x} = 3\times10^5$, varies from 200 to 250 over the Mach number

range covered here. This value compares closely with results of other experimental work on boundary-layer transition on blunt noses, for example, reference 5. The possibility of the flow undergoing a turbulent-to-laminar transition as a result of expansion at the corner would have some influence on this conclusion. However, the evidence presented here does not appear to support such a possibility (see appendix).

The curve shown in figure 10 employs the criterion of $R_{2_x} = 3\times10^5$ for the onset of turbulent flow on the face. The Reynolds number, R_{2_d}, at which R_{2_x} will just equal 3×10^5 at the leeward corner is plotted against angle of attack. Turbulent flow on the front face will occur first along the leeward meridian. The maximum value of R_{2_d} for laminar flow on the face is 5.7×10^5 at $\alpha = 0°$.

CONCLUDING REMARKS

An investigation was conducted on an Apollo-like bluff body to determine the influence of the flight environment on the boundary-layer separation and transition characteristics in the afterbody flow. The following trends and features were observed:

1. Within the range of test conditions, the flow separation and reattachment behavior on the afterbody were found to be sensitive primarily to Mach number and angle of attack. There appeared to be no effect of Reynolds number in the laminar flow regime; however, at the highest Reynolds numbers the flow was turbulent and showed attached afterbody flow even at small angles of attack.

2. Laminar flow in the separated boundary layer occurred below a Reynolds number of around 3×10^5 (based on the flow conditions downstream of the normal shock wave and the streamline distance from the stagnation point to the front-face edge).

3. The streamline distance to transition in the separated afterbody flow, measured from the stagnation point, normalized with respect to the model diameter, and plotted as a function of Reynolds number, correlates all the data of this investigation at all angles of attack. This distance, as expected, decreases with increasing Reynolds number, based on normal-shock conditions and model diameter.

Ames Research Center
National Aeronautics and Space Administration
Moffett Field, California, 94035, May 2, 1968
129-01-09-04-00-21

APPENDIX

CRITERIA USED FOR INTERPRETING SHADOWGRAPHS

The existence of a laminar or turbulent boundary layer on the face of a bluff body at given free-stream conditions has been a subject of some controversy in the past. Since the model-face image in shadowgraph may be obscured by the optical distortion produced by the bow shock wave, the boundary layer on the face usually cannot be observed directly. It has been found (see refs. 3 and 6) that certain features in shadowgraphs indicate turbulence on the face of flat-faced bodies. These features have been described as "filaments of light" and are seen in the shadowgraphs as thin streaks projecting into the model shadow from the model front-face profile. The filaments are so fine that they do not reproduce well in half tones; figure 11, a half-tone print of a typical shadowgraph from the present investigation, indicates their presence.

The objectives of this appendix are (1) to confirm insofar as possible the validity of filaments as turbulence indicators and (2) to use them in conjunction with visible features in the separated flow to develop criteria for determining boundary-layer transition in or ahead of the separated boundary layer.

To accomplish these objectives, shadowgraphs of models in flight with boundary-layer trips on the face were studied. The models were 3 cm in diameter and had three types of trips. Type I was an annular, V-shaped groove of 60° included angle, the groove was 0.025 cm deep, and was placed midway between the center and corner. Type II had seven concentric grooves of the same geometry as type I, spaced at 0.2-cm increments from the center. Type III had No. 80 carborundum grit uniformly distributed over the face. The models were launched at a Mach number of 2.8 and a Reynolds number, R_{2_d}, of either 0.35 or 1.05 million.

The influence of boundary-layer trips on the separated boundary layer downstream of the model corners can be seen in figure 12. The shadowgraph of a model with no boundary-layer trips (fig. 12(a)) has no filaments of light, thus indicating the boundary layer on the model face is laminar. The separated boundary layer downstream of the model corners is laminar approximately one-half model diameter along the windward meridian and one-third model diameter along the leeward meridian, and appears as a smooth even line. In the inviscid region downstream of transition, there are unsteady waves created by eddies in the turbulent boundary layer. Forward of transition no waves can be seen emanating from the laminar portion of the separated boundary layer. The region between the laminar portion of the separated boundary layer and model afterbody profile appears much less disturbed than that farther downstream over the afterbody. This is further evidence of a laminar separated boundary layer.

The separated boundary layer is a sharply defined line downstream of the model corners, partly because of the density profile of the mixing layer. The light refraction by the mixing layer causes underexposure along the low-density edge (the outboard edge) and overexposure along the high-density edge. (The underexposed line at the model is a diffraction fringe.) Three-dimensional eddies would cause a granular image and make the distinct image appear irregular or fuzzy. Immediately after the expansion at a corner, however, the turbulent velocities are small compared to the flow velocities, and the eddies themselves have been greatly stretched along the local flow direction so that the presence of turbulence is difficult to detect optically, suggesting that in this flow region the onset of turbulence is probably forward of the point at which it can first be observed.

For the model with type I boundary-layer trip (fig. 12(b)), there were filaments of light near the corners along the front-face profile; but they were very fine and somewhat difficult to detect. They indicate, however, that the flow near the corner was not laminar. Turbulence in the separated boundary-layer profile is observed farther upstream than that in figure 12(a). Unsteady waves in the inviscid region are generated by this turbulence. The eddies inboard of the separated boundary-layer profile extend virtually to the corner, indicating that the flow is at least transitional in this region. For the flow conditions of figure 12(b) transition may have begun ahead of the corner and continued past the corner even in the presence of the strong local expansion field at the corner.

For the model with the type II trip, the filaments of light were strong. There also were waves from the front face that appeared to fill the subsonic shock layer and could be a resonant standing wave system associated with the boundary-layer trips. The waves in themselves do not necessarily assure the existence of a turbulent boundary layer on the face although it is obvious that the flow is severely disturbed. But the filaments of light were more apparent in this shadowgraph than in figure 12(b), and the separated boundary layer downstream of the corners appears completely turbulent. Unsteady waves in the inviscid region and turbulent eddies in the inboard region can also be seen as far forward as the corner. The indications are that transition was complete ahead of the corner.

The model in figure 12(d) had a type II trip also; however, the Reynolds number was greater by a factor of 3. The features seen in figure 12(c), that is, waves from the front face, filaments of light, turbulent eddies in the inboard region, unsteady waves in the inviscid region, are more pronounced in figure 12(d). It is similarly concluded that transition was complete ahead of the corner.

The filaments of light in the shadowgraphs of the models with type III trip (fig. 12(e)) were more heavily concentrated than in the shadowgraphs of the other models. They were continuous from corner to corner, indicating that a turbulent boundary layer virtually covers the front face. Downstream of the upper corner the separated boundary layer appears turbulent. There are unsteady waves in the inviscid region and turbulent eddies fill the inboard region. Downstream of the lower corner the separated boundary layer appears

laminar for a very short distance. The absence of unsteady waves and turbulent eddies in the inviscid and inboard regions indicates at most a briefly laminar boundary layer. The differences between the upper and lower profiles are possibly due to the boundary layer being thinner along the lower meridian of the face. The separated boundary layer downstream of the corners in figure 12(b), and downstream of the lower corner in figure 12(e), appeared laminar for a short distance even though filaments of light indicated a turbulent boundary layer ahead of the corner. Reference 7 shows that it is possible for a rapid expansion to make a turbulent boundary layer temporarily laminar. The turbulent eddy velocities may be made negligible by the expansion. If the Reynolds number is low enough (according to ref. 7), the flow may remain laminar; if not, it becomes turbulent. The latter is expected to be the situation in the present tests.

From observations such as those described here, the following criteria were used as a basis for interpreting the shadowgraphs of this investigation:

1. Narrow filaments of light projected into the model shadow from the front-face profile indicate a turbulent boundary layer.

2. Unsteady waves in the inviscid region and turbulence eddies in the inboard region of the wake indicate a turbulent separated boundary layer.

REFERENCES

1. Chapman, Gary T.; and Jackson, Charles T., Jr.: A Free-Flight Investigation of the Heat Transfer and Afterbody Flow Field of an Apollo-Type Configuration at Speeds to 10,000 Ft/Sec. NASA TM X-853, 1963.

2. Intrieri, Peter F.: Effects of Transverse Center-of-Gravity Displacement, Afterbody Geometry, and Front-Face Curvature on the Aerodynamic Characteristics of Mercury-Type Models at a Mach Number of 5.5. NASA TM X-569, 1961.

3. Canning, Thomas N.; and Sommer, Simon C.: Investigation of Boundary-Layer Transition on Flat-Faced Bodies of Revolution at High Supersonic Speeds. NACA RM A57C25, 1957.

4. Sommer, Simon C.; Short, Barbara J.; and Compton, Dale L.: Free-Flight Measurements of Static and Dynamic Stability of Models of the Project Mercury Re-entry Capsule. NASA TM X-373, 1960.

5. Stetson, K. F.: Boundary Layer Transition on Blunt Bodies With Highly Cooled Boundary Layers. J. Aero. Sci., vol. 27, no. 2, Feb. 1960, pp. 81-91.

6. Seiff, Alvin; Sommer, Simon C.; and Canning, Thomas N.: Some Experiments at High Supersonic Speeds on the Aerodynamic and Boundary-Layer Transition Characteristics of High-Drag Bodies of Revolution. NACA RM A56I05, 1957.

7. Sternberg, Joseph: The Transition From a Turbulent to a Laminar Boundary Layer. BRL Rep. 906, Ballistic Res. Lab., Aberdeen Proving Ground, Md., May 1954.

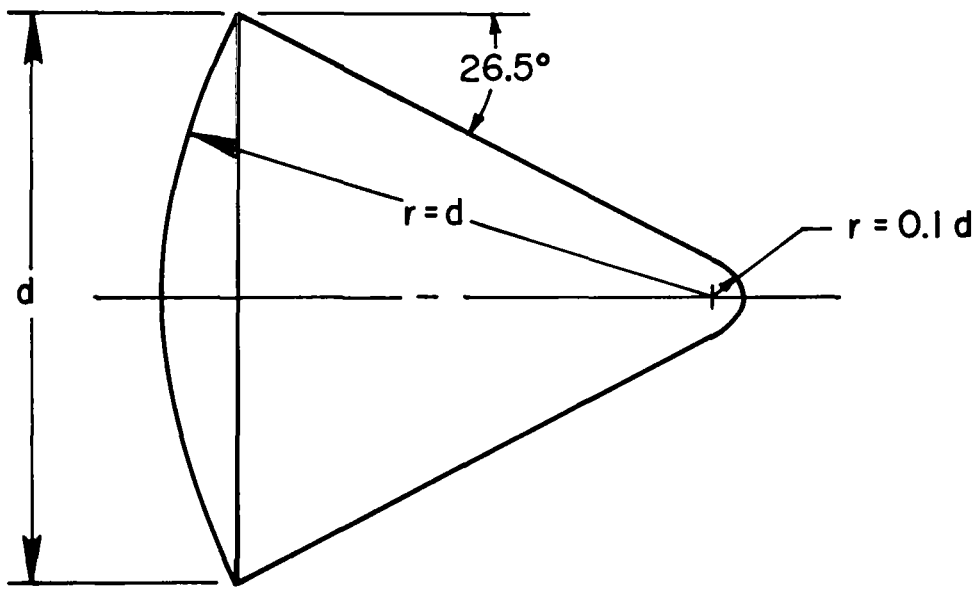

Figure 1.- Model configuration.

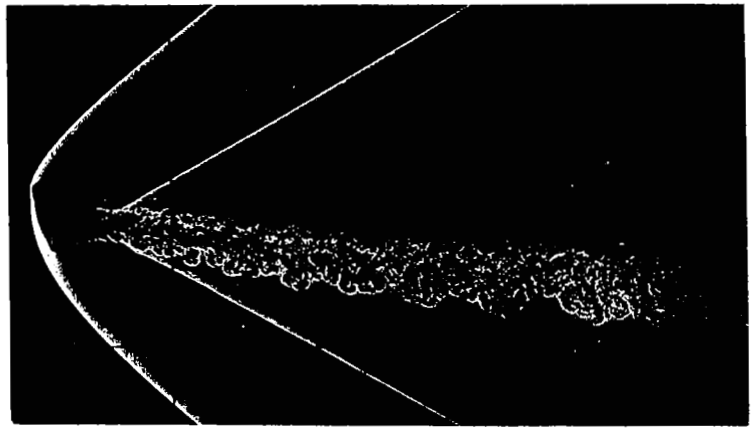

(a) $M = 2$; $\alpha = 22^{\circ}$, $R_{\infty d} = 0.45 \times 10^6$,
windward $R_{2_x} = 0.39 \times 10^5$,
leeward $R_{2_x} = 2.93 \times 10^5$.

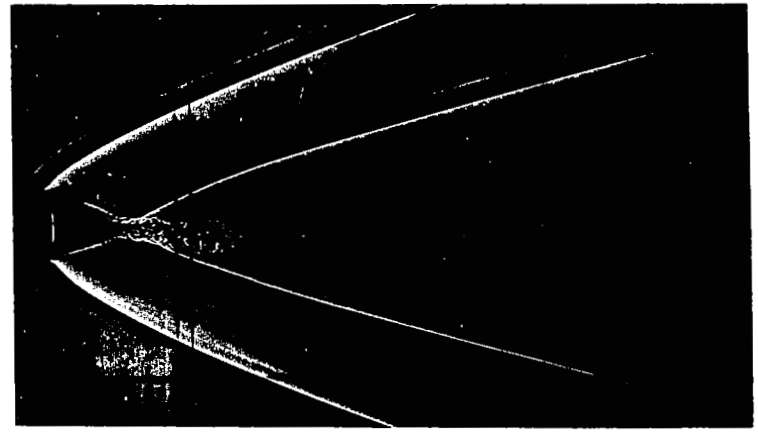

(c) $M = 4$; $\alpha = 8^{\circ}$, $R_{\infty d} = 0.9 \times 10^6$,
windward $R_{2_x} = 1.43 \times 10^5$,
leeward $R_{2_x} = 2.42 \times 10^5$.

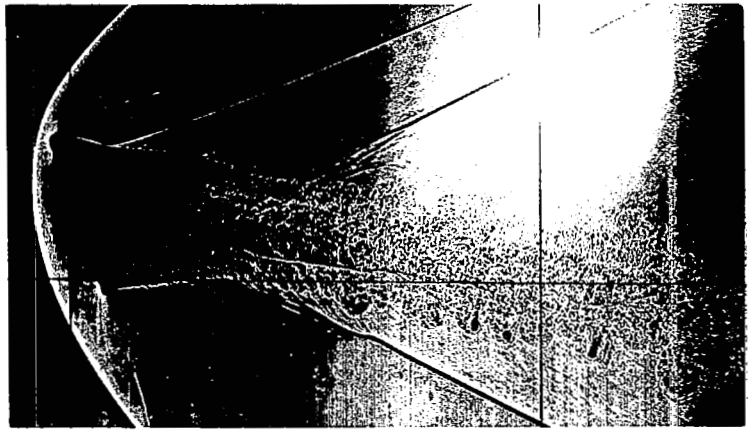

(b) $M = 2$; $\alpha = 22^{\circ}$, $R_{\infty d} = 1.4 \times 10^6$,
windward $R_{2_x} = 1.40 \times 10^5$,
leeward $R_{2_x} = 8.39 \times 10^5$.

(d) $M = 4$; $\alpha = 8^{\circ}$, $R_{\infty d} = 2.7 \times 10^6$,
windward $R_{2_x} = 4.15 \times 10^5$,
leeward $R_{2_x} = 7.11 \times 10^5$.

AAA-169-3

Figure 2.- Effect of Reynolds number on near-wake flow.

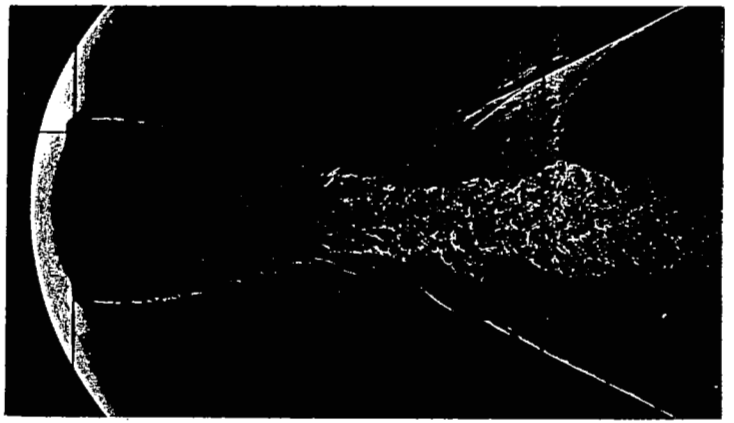

(a) $\alpha = 3^{\circ}$

(c) $\alpha = 15^{\circ}$

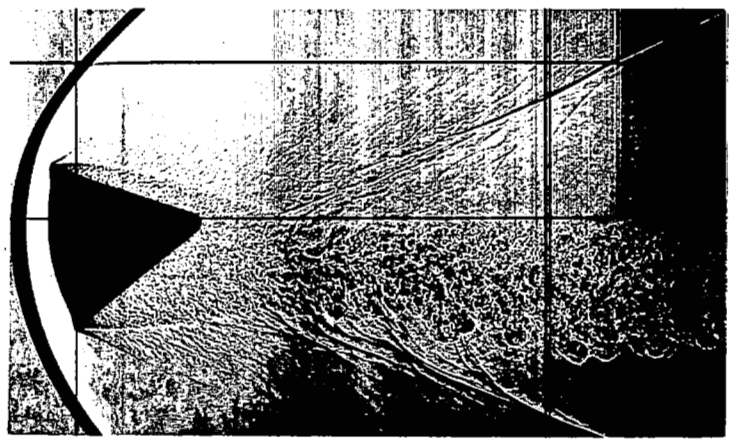

(b) $\alpha = 10^{\circ}$

AAA-169-2

(d) $\alpha = 25^{\circ}$

Figure 3.- Effect of angle of attack on near-wake flow; $M = 2.2$, $R_{\infty d} = 1.5 \times 10^{6}$.

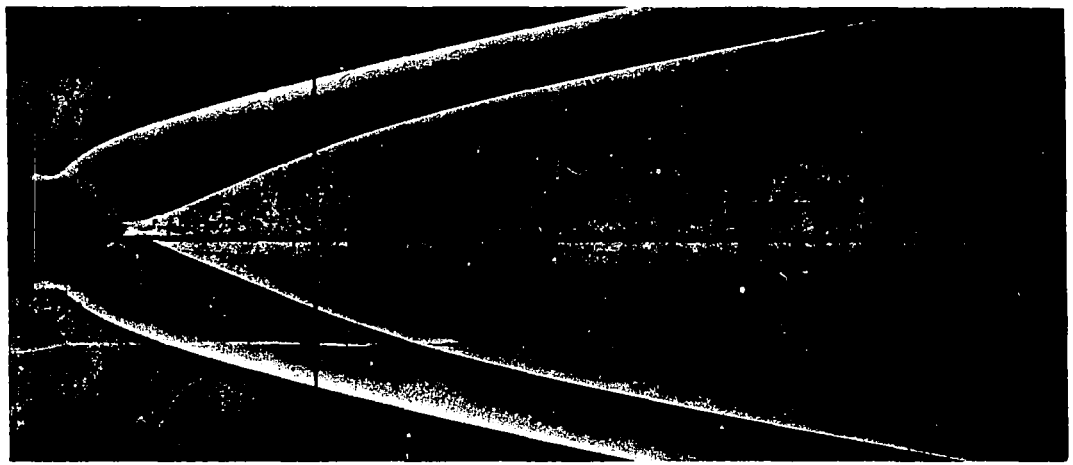

(a) M = 8.75; $R_{\infty d}$ = 4.23×10^6

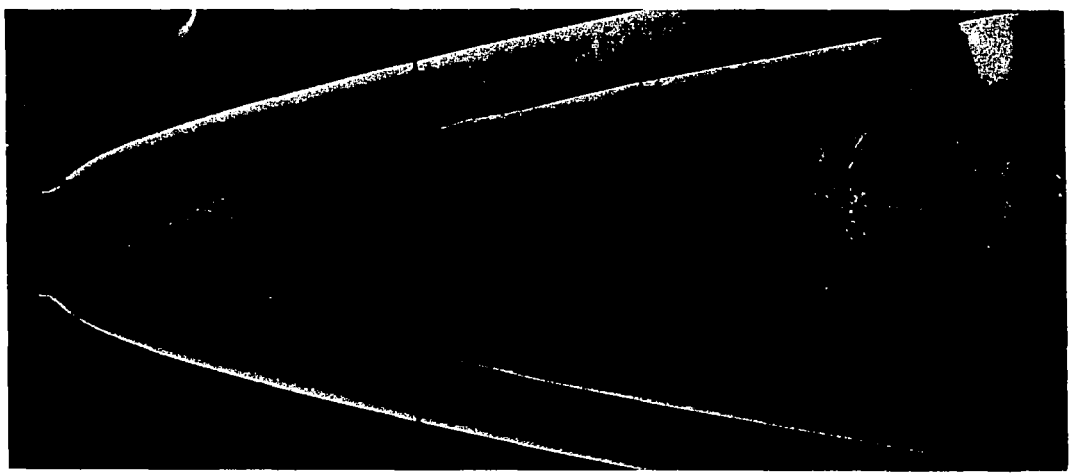

AAA-169-1

(b) M = 8.28; $R_{\infty d}$ = 3.09×10^6

Figure 4.- Attached and separated flow on afterbody; $\alpha \approx 0^{\circ}$.

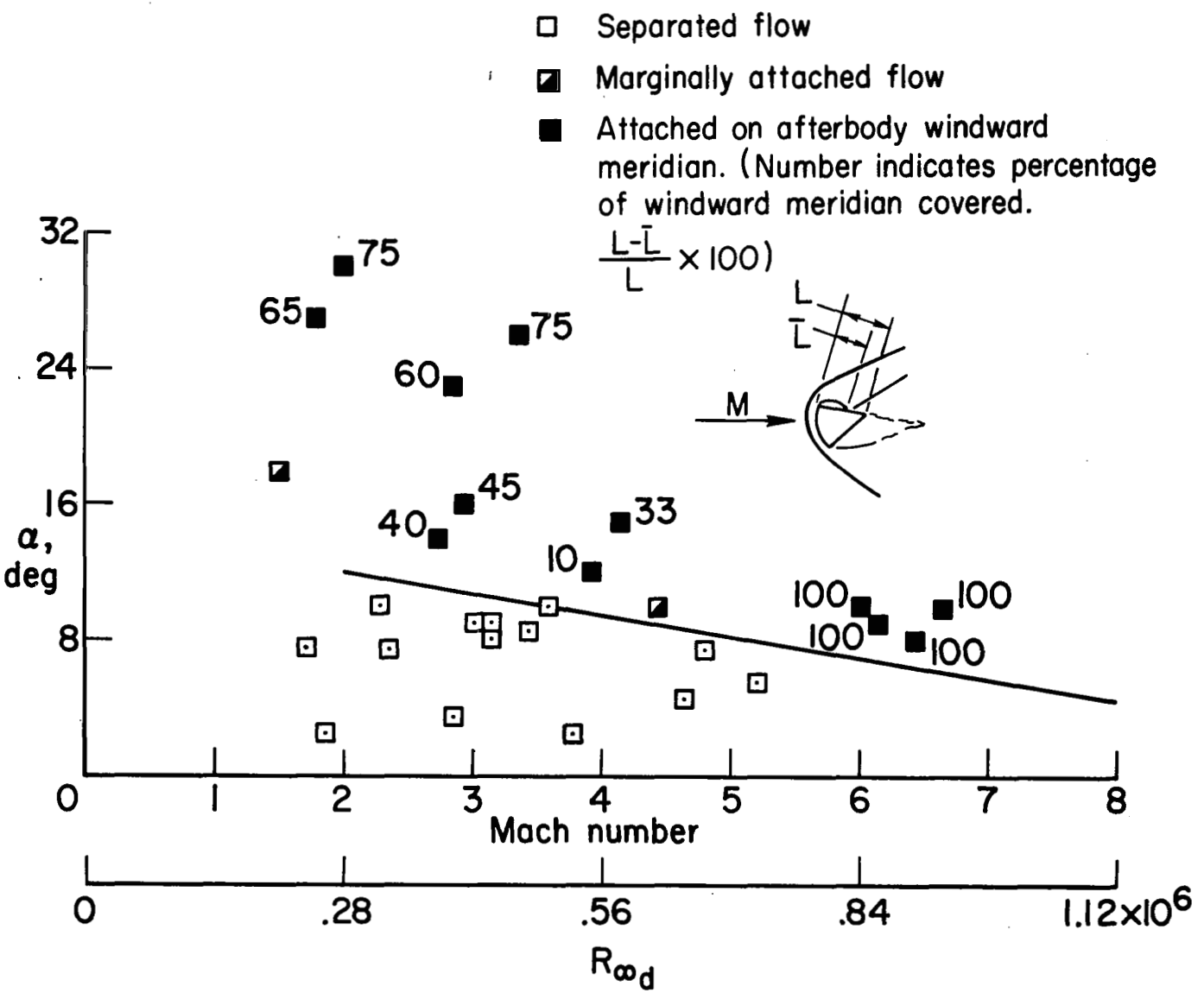

(a) d = 0.63 cm; p = 1 atm (ref. 1).

Figure 5.- Flow on afterbody windward meridian.

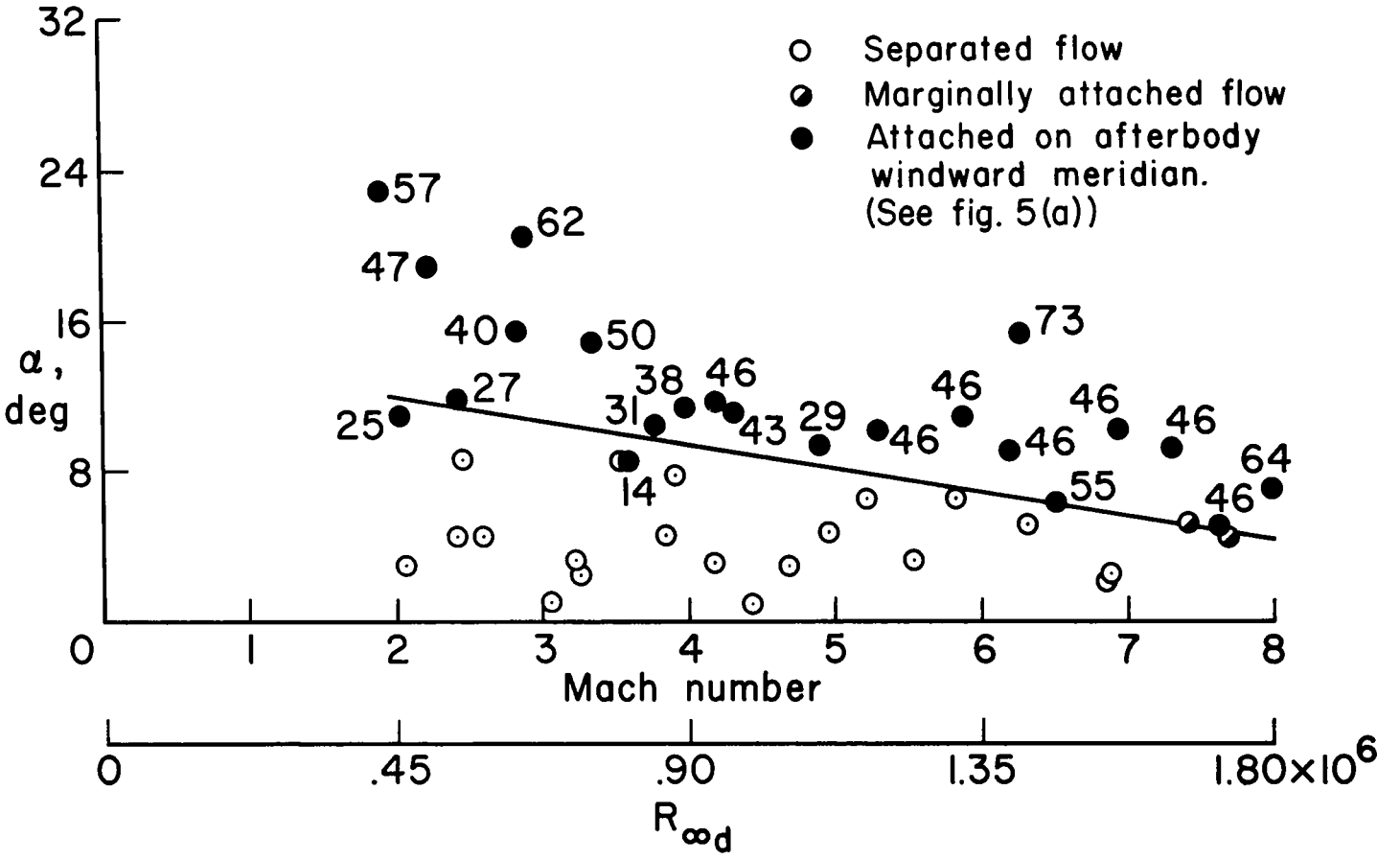

(b) d = 1 cm; p = 1 atm

Figure 5.- Continued.

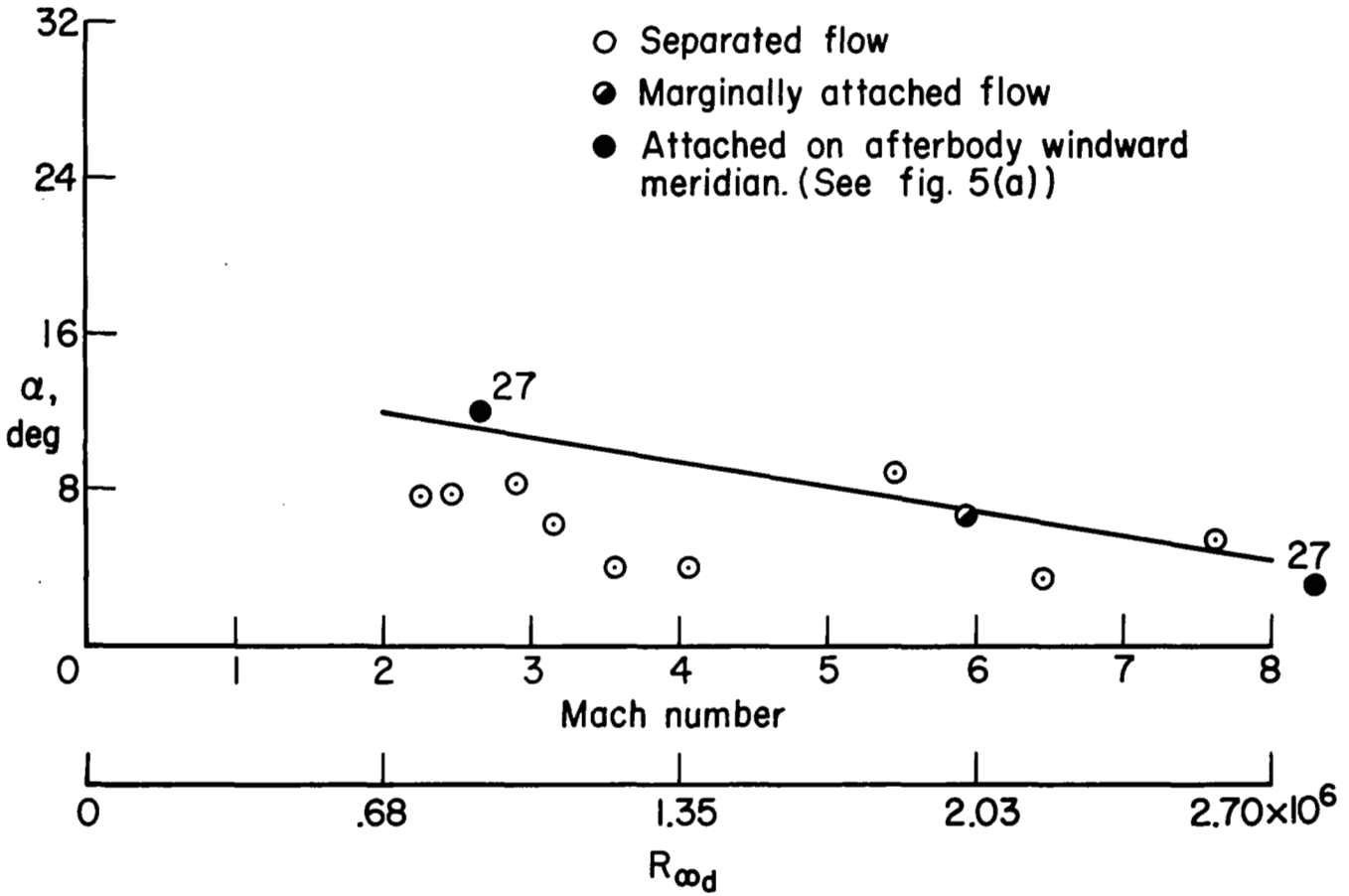

(c) d = 1 cm; p = 1-1/2 atm

Figure 5.- Continued.

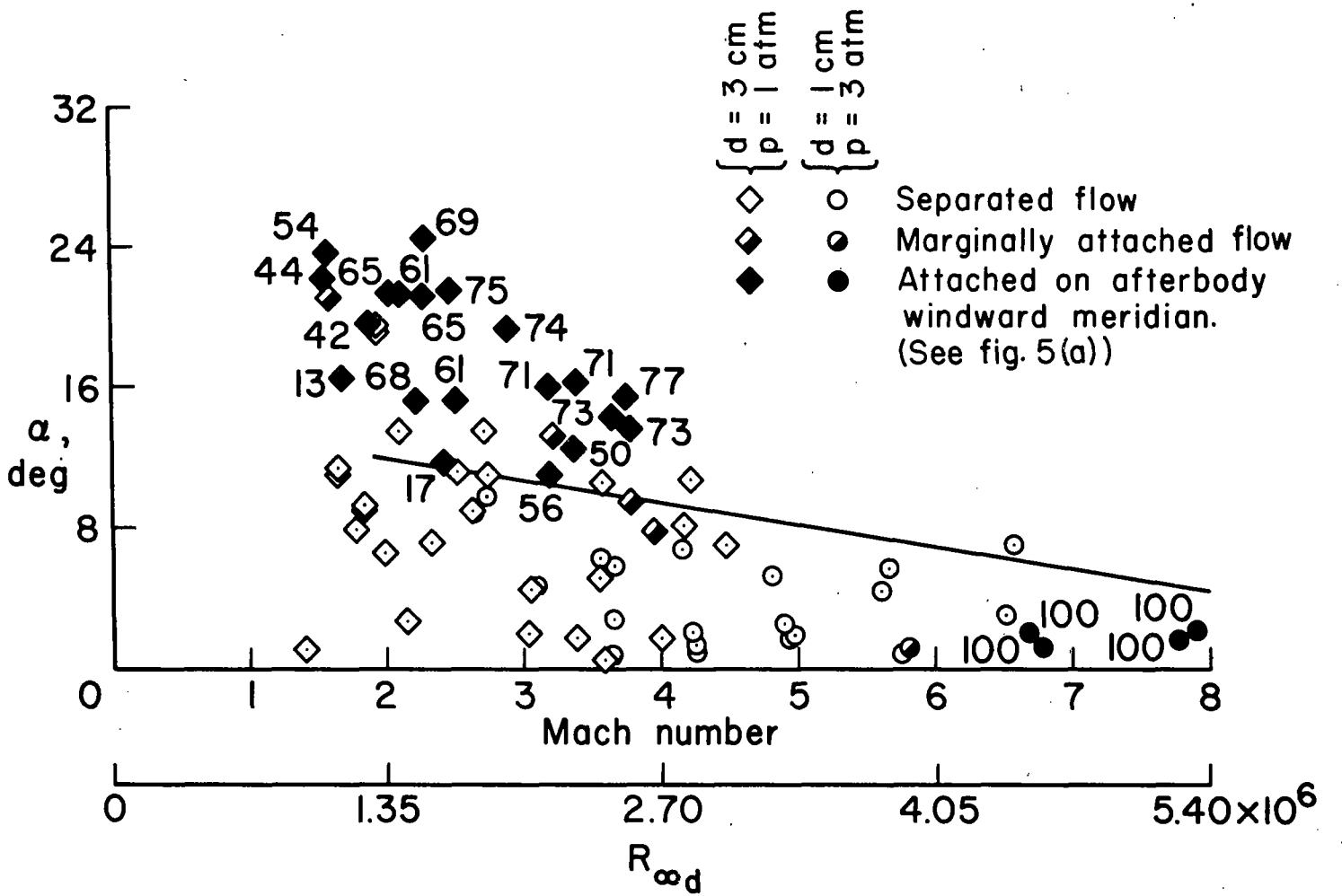

(d) d = 3 cm, p = 1 atm; and d = 1 cm, p = 3 atm

Figure 5.- Concluded.

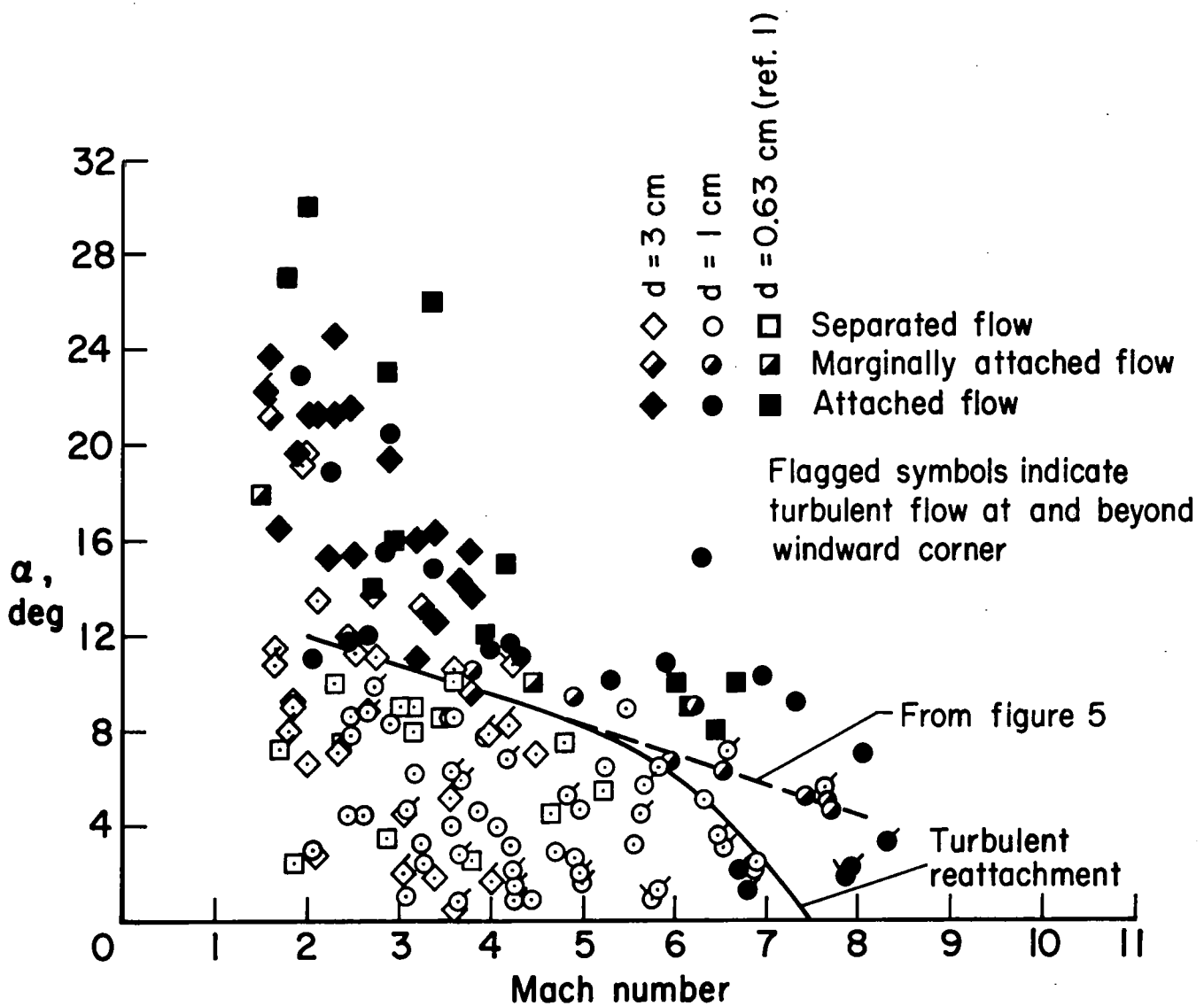

Figure 6.- Flow conditions and reattachment on afterbody windward meridian.

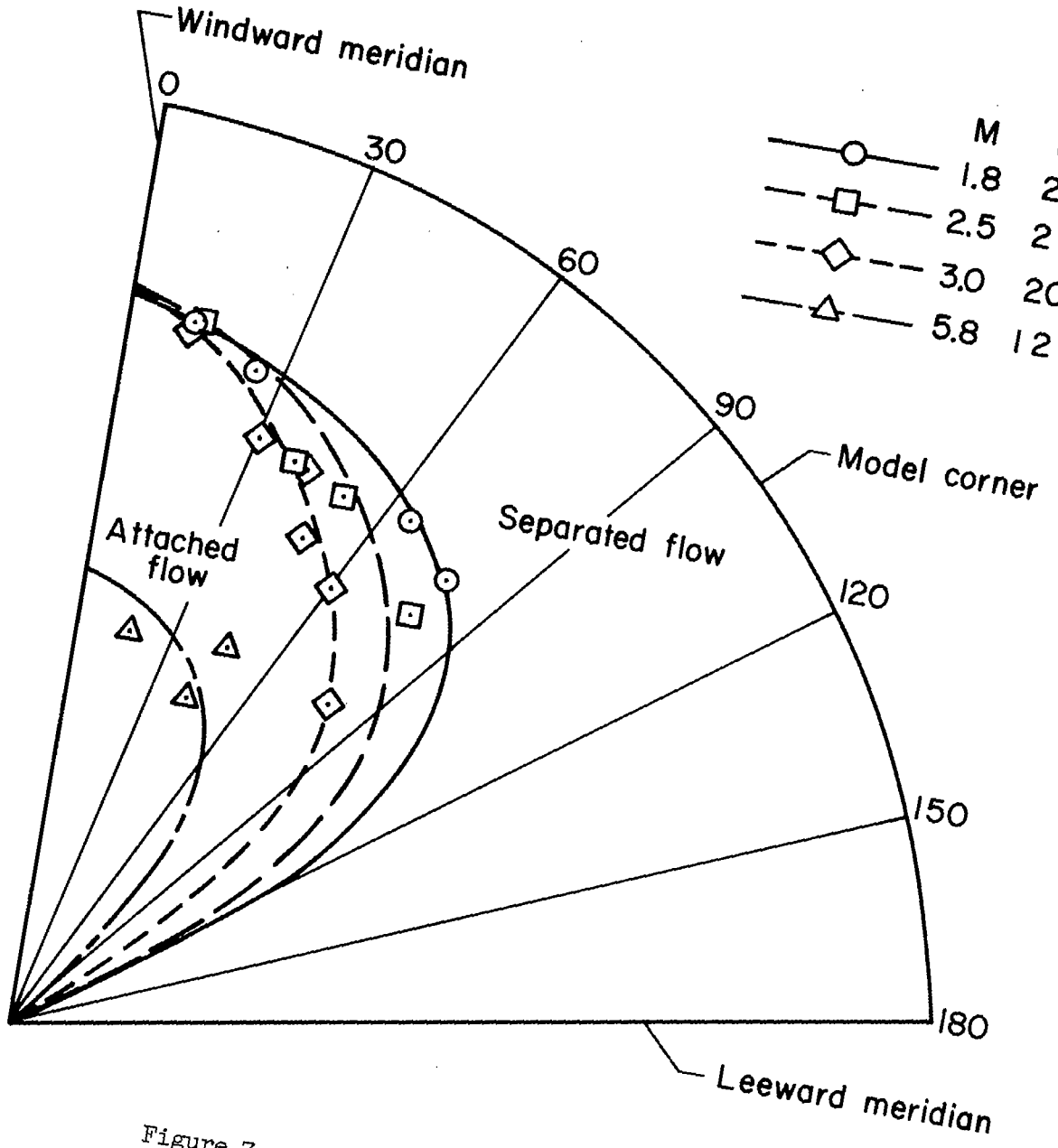

Figure 7.- Afterbody reattachment patterns.

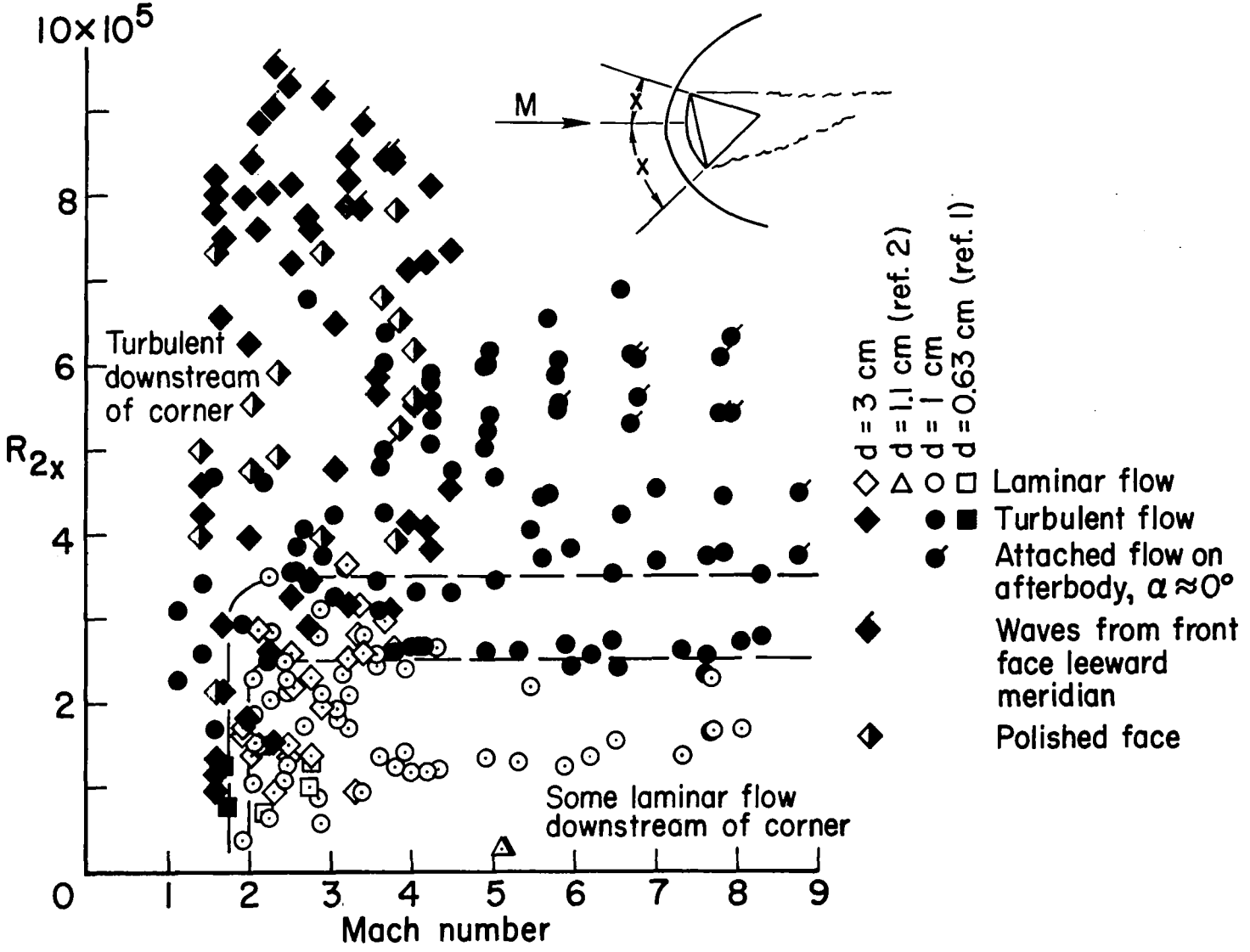

Figure 8.- Condition of flow downstream of model corner.

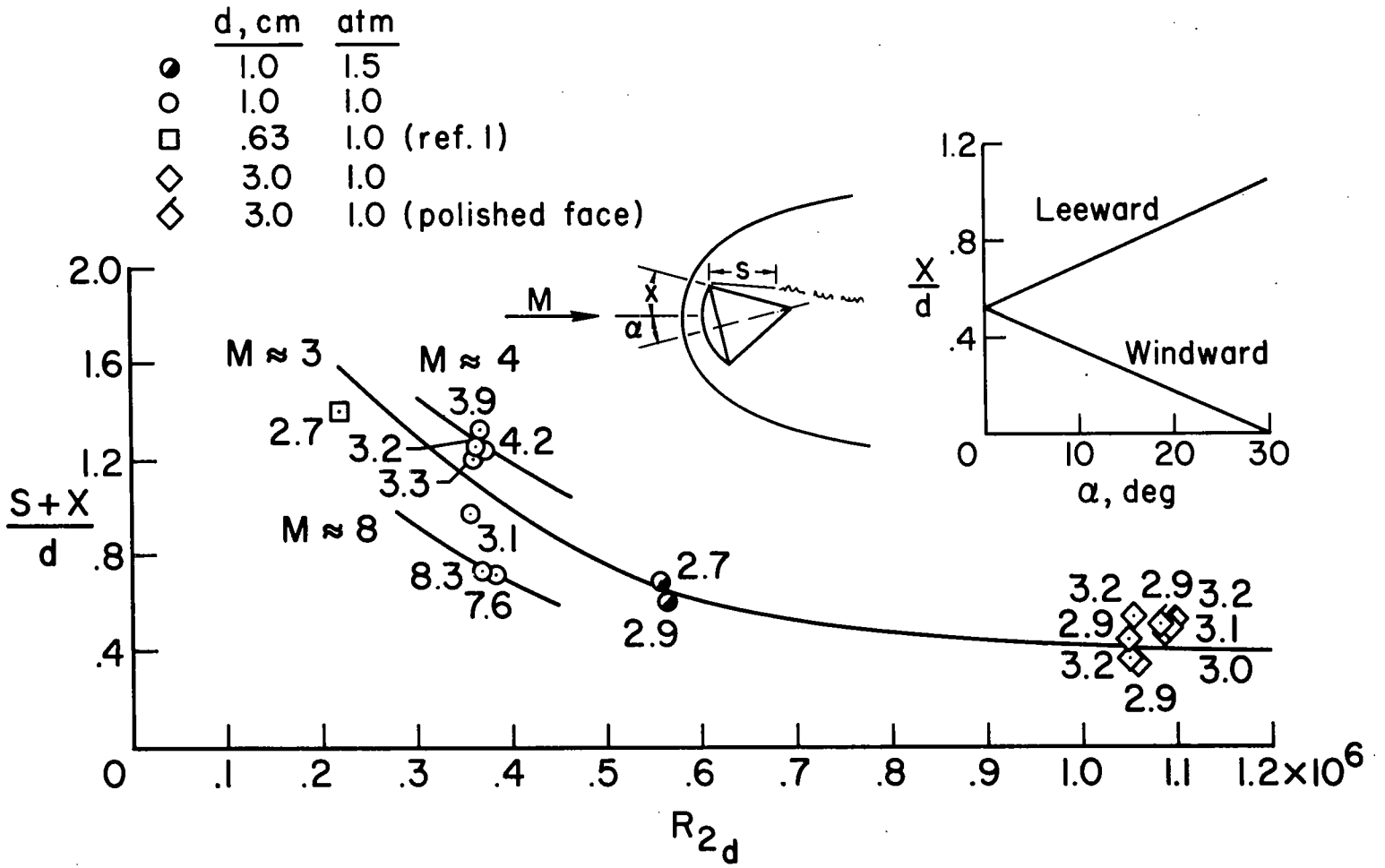

Figure 9.- Extent of laminar flow in separated region behind base.

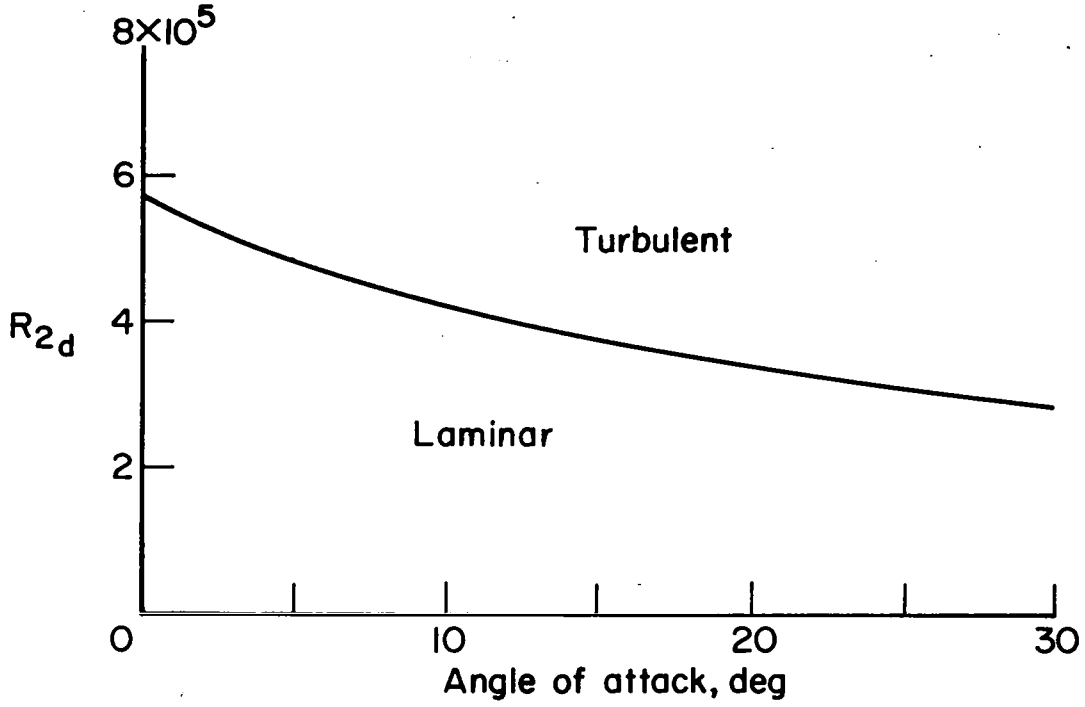

Figure 10.- Predicted limiting value for laminar flow on the face leeward meridian.

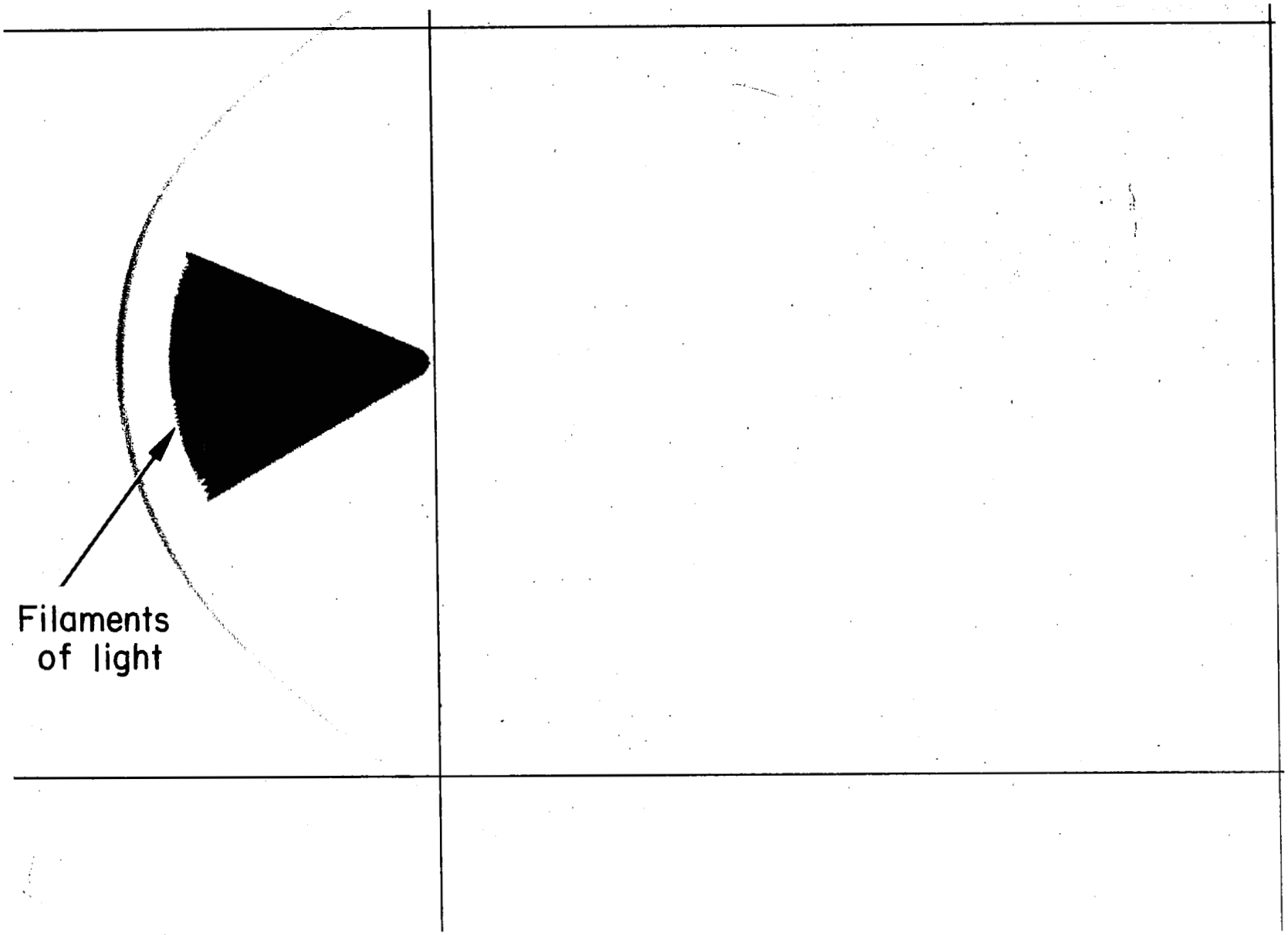

Figure 11.- Indicator of turbulence on model front face.

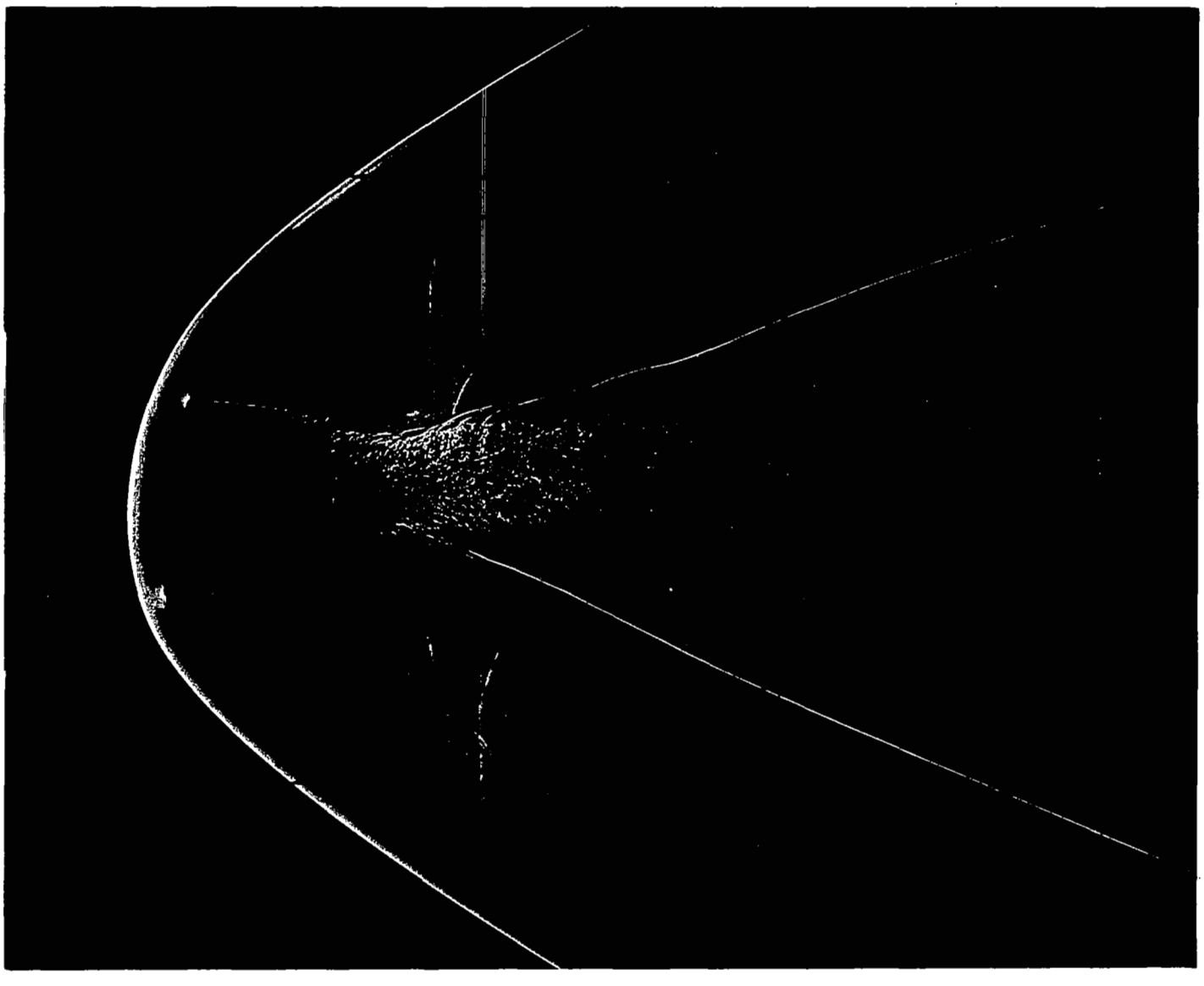

A-40620

(a) No trip; M = 2.8, R_{2_d} = 0.35x10^6

Figure 12.- Flow field around models with and without boundary-layer trips on the face.

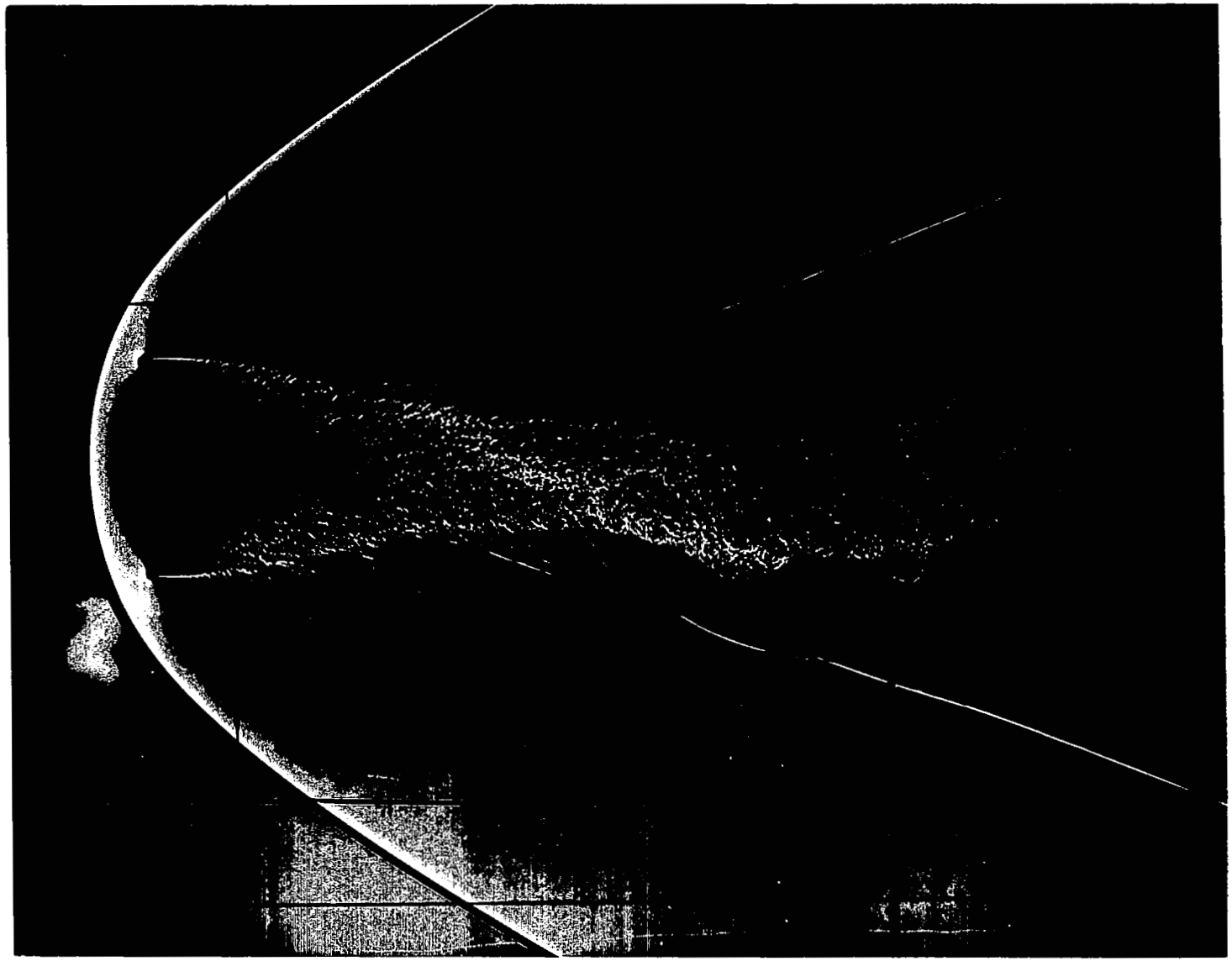

A-40619

(b) Type I trip; M = 2.8, R_{2d} = 0.35x10^6

Figure 12.- Continued.

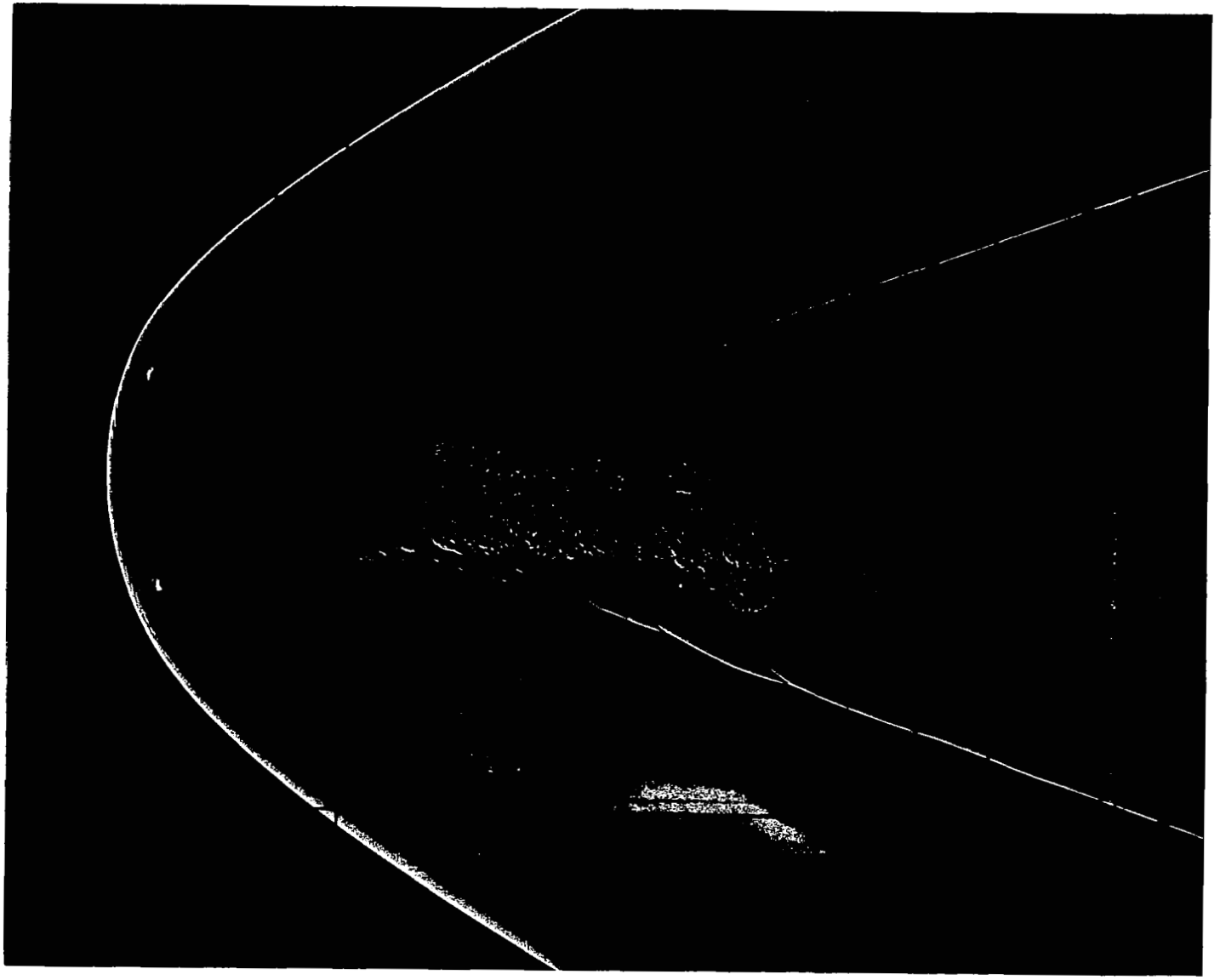

A-40618

(c) Type II trip; M = 2.8, $R_{2_d} = 0.35 \times 10^6$

Figure 12.- Continued.

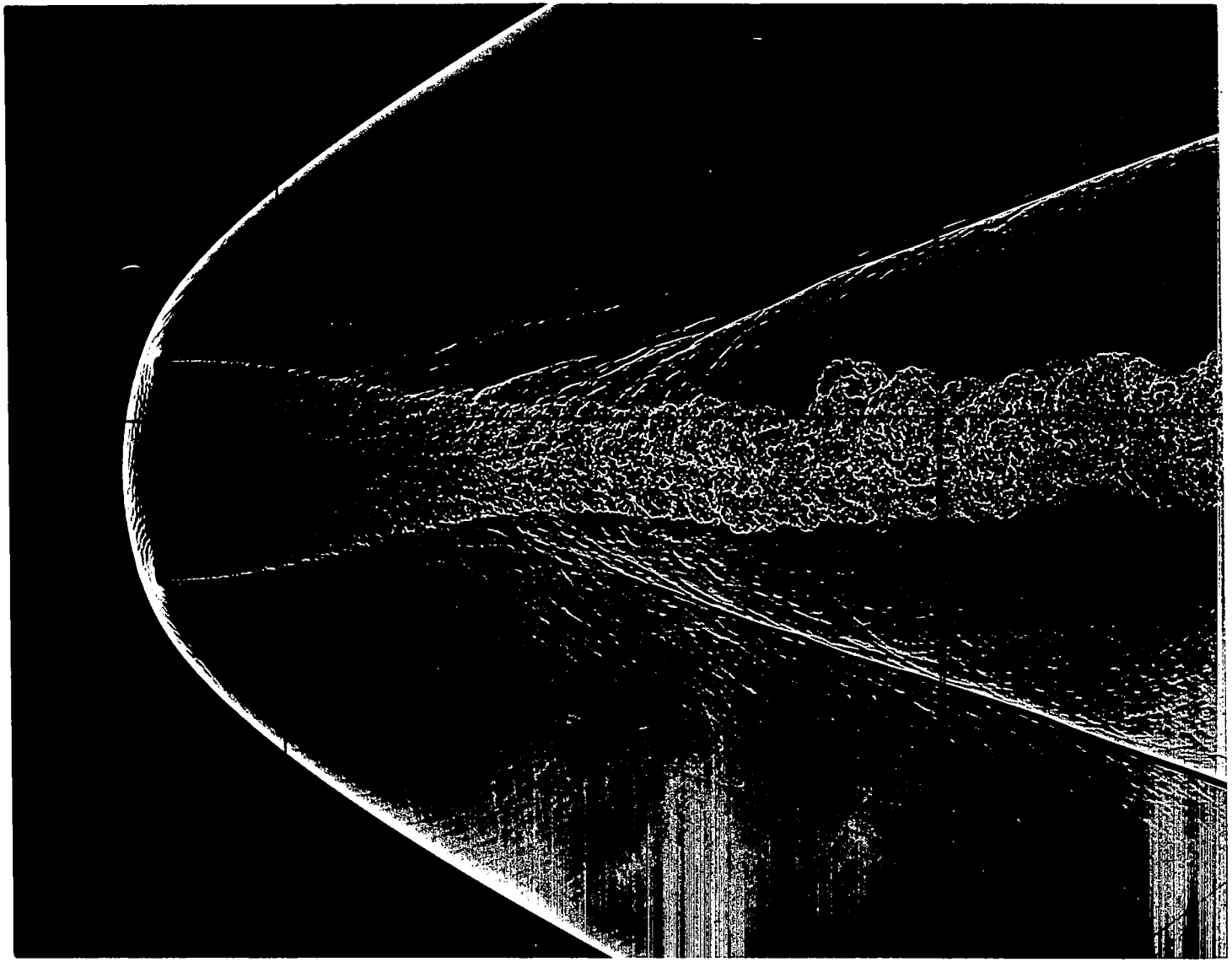

A-40622

(d) Type II trip; M = 2.8, R_{2_d} = 1.05x10^6

Figure 12.- Continued.

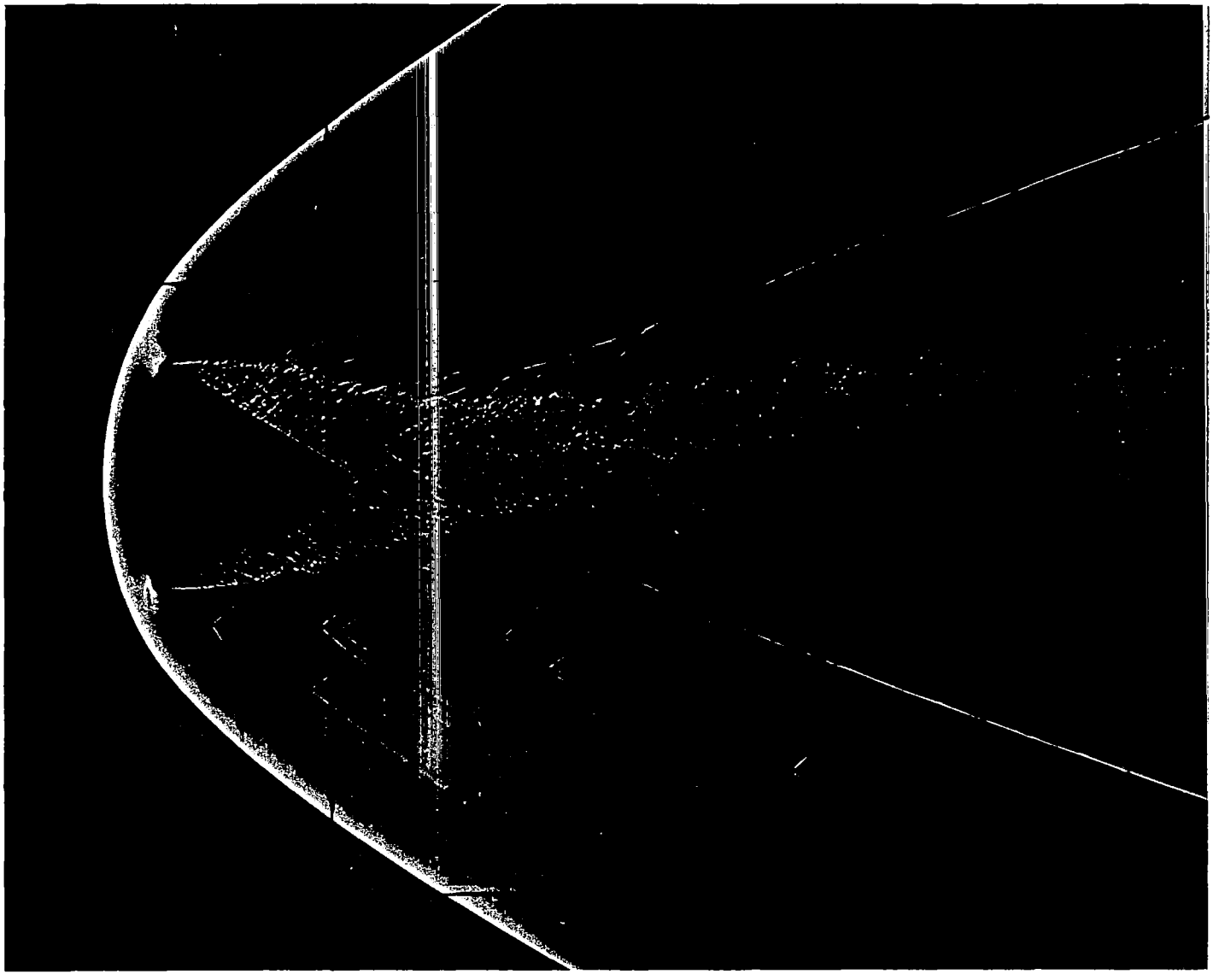

A-40621

(e) Type III trip; M = 2.8, $R_{2_d} = 0.35 \times 10^6$

Figure 12.- Concluded.